ANNALS OF GEOPHYSICS, 59, Fast Track 5, 2016 DOI: 10.4401/ag-7201

Preliminary analysis of the accelerometric recordings of the August 24th, 2016 M_W 6.0 Amatrice earthquake

GIOVANNI LANZANO*, LUCIA LUZI, FRANCESCA PACOR, RODOLFO PUGLIA, MARIA D'AMICO, CHIARA FELICETTA, EMILIANO RUSSO

Istituto Nazionale di Geofisica e Vulcanologia, Milan, Italy
* giovanni.lanzano@ingv.it

Abstract

On 24 August 2016, at 1.36:32 GMT, a M_w 6.0 earthquake with epicenter located below the village of Accumoli, struck a wide area among the boundaries of Lazio, Abruzzo, Umbria and Marche regions (Central Italy): the main event caused the collapse of several buildings and about 300 fatalities, mainly in the towns of Amatrice, Arquata del Tronto and Accumoli. The main event was recorded by about 350 sensors, belonging to the Italian Accelerometric Network (Rete Accelerometrica Nazionale, RAN) operated by the Department of Civil Protection (DPC), the Italian Seismic Network (Rete Sismica Nazionale, RSN) managed by the Istituto Nazionale di Geofisica e Vulcanologia (INGV), and to other local networks. All the corrected data are available at the Engineering Strong Motion Database (esm.mi.ingv.it). This paper reports the preliminary results of the analysis of the strong-motion recordings.

I. INTRODUCTION

On 24 August 2016, at 1.36:32 GMT, a M_W 6.0 (INGV-CNT Seismic Bulletin) earthquake with epicenter located below the village of Accumoli, struck a wide area among the boundaries of Lazio, Abruzzo, Umbria and Marche regions (Central Italy). The epicenter is located below the village of Accumoli (Latitude 42.70°, Longitude 13.23°, Depth 8.1km, INGV-CNT Seismic Bulletin) and the fault plane solution (TDMT, CNT) indicates normal faulting, which is in agreement with the prevailing tectonic style of the area (according to the seismogenic zonation ZS9, Meletti et al. 2008). The fault geometry was calculated by Tinti et al. (2016) and has the following characteristics: strike 156°, dip 50°, rake -85°, length 26km, width 16km.

The Italian Accelerometric Network (RAN), managed by the Department of Civil Protection (DPC), the Italian seismic network (RSN), managed by the Istituto Nazionale di Geofisica e Vulcanologia (INGV) and other regional networks (e.g, managed by OGS and AMRA) provided the records of the mainshock.

The unprocessed records are available at ran.protezionecivile.it/IT/index.php for the RAN network and at the European Integrated Data Archive (EIDA, www.orfeus-eu.org/data/eida) for the RSN and other Italian and European networks (e.g, Croatian and French seismic networks). The processed records are available at the Engineering Strong-Motion database website (ESM, esm.mi.ingv.it, Luzi et al. 2016) and the Italian Accelerometric Archive (ITACA, itaca.mi.ingv.it, Luzi et al. 2008; Pacor et al. 2011). About 350 waveforms were manually processed using the procedure detailed in Pacor et al. (2011). The earthquake was over-

all recorded by 14 stations within 30km and 42 within 50km from the epicenter.
The location of the epicenter, the surface projection of the causative fault and the spatial distribution of the recording stations is shown in Figure 1.

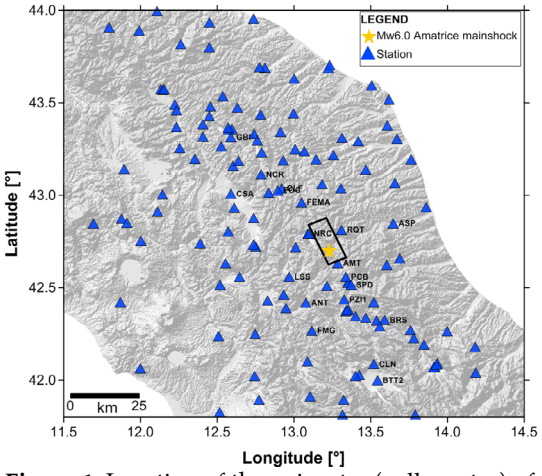

Figure 1. Location of the epicenter (yellow star) of the Amatrice (M_w 6.0) earthquake and distribution of the recording stations (blue triangles). The surface projection of the causative fault by Tinti et al. (2016) is also shown.

II. Spatial distribution of the ground motion

The spatial distributions of the largest horizontal component of the recorded ground motion for peak ground acceleration PGA and velocity PGV are given in Figure 2 and 3. PGAs larger than 300cm/s^2 were recorded at the near-source RAN stations RQT (Arquata del Tronto, R_{JB} = 4.6km, EC8-B, PGA = 437cm/s^2), AMT (Amatrice, R_{JB}=1.4km, EC8-B, PGA = 425cm/s^2), NRC (Norcia, R_{JB}=2.0km, $V_{S,30}$ = 687 m/s, PGA = 396cm/s^2) and PCB (Poggio Cancelli, R_{JB}=10.7km, EC8-B, PGA = 302cm/s^2). Values larger than 200 cm/s^2 were also observed in the NW direction at distance larger than 30km from the epicentre, for stations FOC (Foligno, R_{JB}=26.3km, EC8-C, PGA = 323cm/s^2), NCR (Nocera, R_{JB}=39.4km, $V_{S,30}$ = 555 m/s, PGA = 218cm/s^2) and FEMA (Monte Fema, R_{JB}=13.9km, EC8-B, PGA = 242cm/s^2).

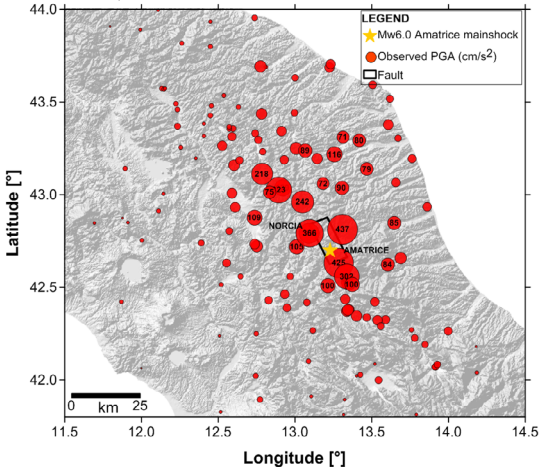

Figure 2. Spatial distribution of the maximum horizontal Peak Ground Acceleration (cm/s^2).

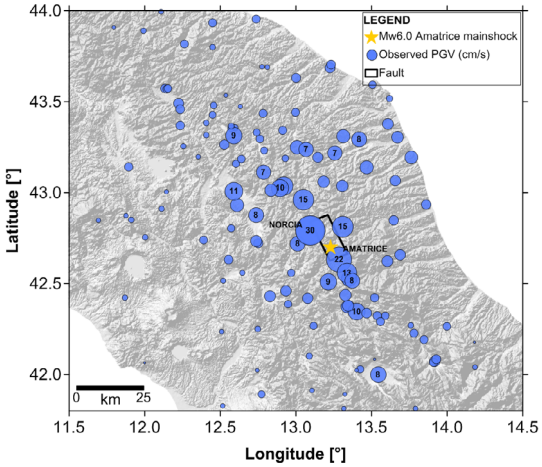

Figure 3. Spatial distribution of the maximum horizontal Peak Ground Velocity (cm/s).

The largest recorded PGVs are about 30cm/s and 27cm/s at stations NRC and NOR, respectively, both located in the sedimentary basin of Norcia. Values higher than 10cm/s were also observed at the near-source stations AMT (PGV = 21.5cm/s), FEMA (PGV = 14.6cm/s), PCB (PGV = 13.1cm/s) and at farther stations located inside intermountain basins, such as CLF (Colfiorito, R_{JB}=26.1km,

$V_{S,30}$ = 145 m/s, PGV = 11.6 cm/s), CSA (Castelnuovo Assisi, R_{JB}=45.2km, EC8-C, PGV = 10.9 cm/s) and FOC (PGV = 10.2 cm/s). Additional values of the ground-motion intensity measures (PGA, PGV, PGD, Significant duration, Arias and Housner intensities) can be also retrieved from the Re-LUIS-INGV Workgroup (2016) report (V5.0).
Figure 4 and 5 show the spatial distribution of the geometrical mean of the two horizontal components for two spectral ordinates (0.3s and 3s). The strong motion parameters were interpolated using the *kriging* algorithm (Davis, 1973), which takes into account the spatial correlation among the recording stations.

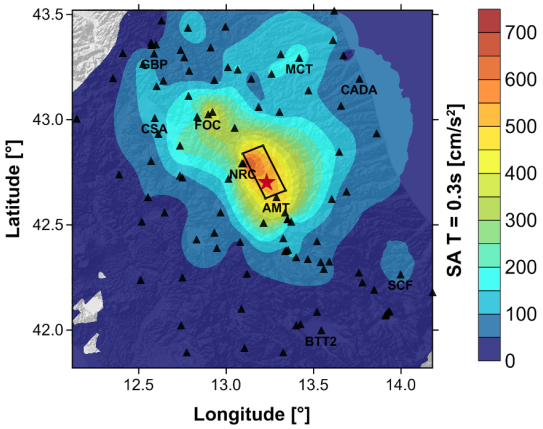

Figure 4. Map of interpolated horizontal spectral acceleration (T = 0.3s).

The maximum values at 0.3s occur inside the surface projection of the fault. The contours are elongated to the NW and the attenuation with distance is asymmetric, with different decay rates with source-to-site azimuth. It might indicate directivity effects due to the rupture propagation along the fault towards the North. The station FOC exhibits higher values compared to other stations with same epicentral distance.
The map of interpolated horizontal spectral acceleration at 3s highlights the low frequency amplifications of the stations located inside alluvial basins (GBP, CSA and BTT2) or along the Adriatic coast (e.g. CADA), due to the presence of surface waves (Bindi et al, 2011b; Di Giulio et al 2003).

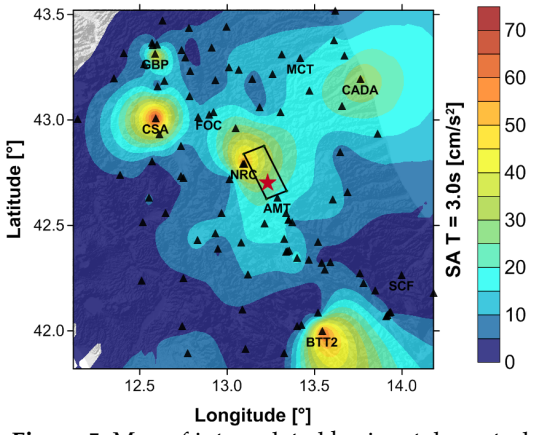

Figure 5. Map of interpolated horizontal spectral acceleration (T = 3s).

III. Comparison of Observed and Predicted Ground Motions

Some ground motion parameters (PGA, PGV and acceleration spectral ordinates at 0.3, 1 and 3 seconds) were compared to the predictions of the most recent GMPEs by Bindi et al (2011a), for Italy (ITA10), and Akkar et al. (2014), for Europe (ASB14). Both GMPEs use the Joyner-Boore distance up to 200km.
Although the selected ground motion models present similar functional forms, they assume different site effect terms: ITA10 accounts for linear soil amplifications through a site term based on Eurocode 8 (EC8; CEN, 2004) soil categories; ASB14 considers $V_{S,30}$ as an explanatory variable for site effects and accounts for non-linear soil amplification through PGA.
Since measured $V_{S,30}$ is available only for 17% of the recording stations, the EC8 soil category for the majority of recording sites was inferred from surface geology (Di Capua et al. 2011). The corresponding $V_{S,30}$ at these sites, was assigned following the Wald and Allen (2007) approach, that adopts the to-

pographic slope as a proxy. In case the $V_{S,30}$ inferred from the slope and the EC8 category from surface geology do not match, the latter was retained and a preferred $V_{S,30}$ is assigned (800 m/s for EC8-A, 580 m/s for EC8-B, 270 m/s for EC8-C, 170 m/s for EC8-D).

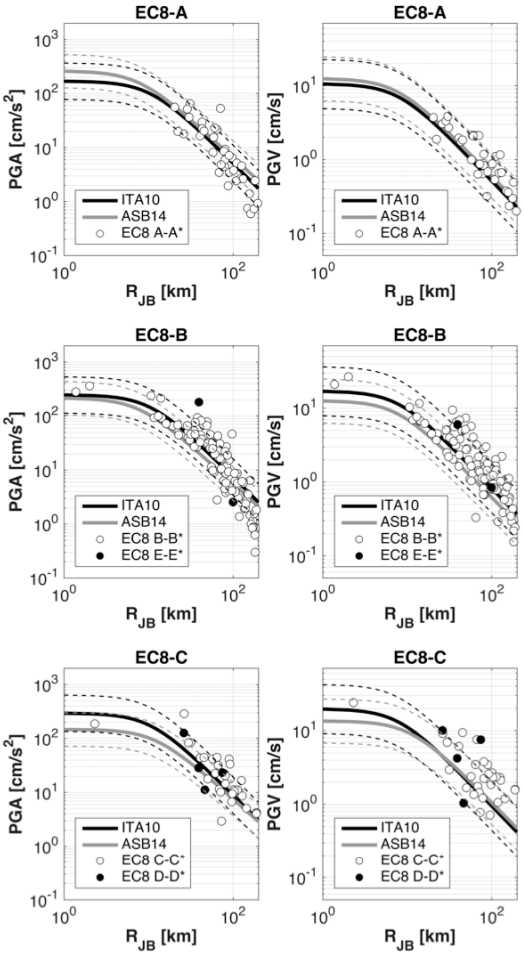

Figure 6. Observation vs. predictions for the geometrical mean of the horizontal components. Left: PGA; right: PGV. Top: EC8-A; middle: EC8-B; bottom: EC8-C. ASB14 predictions are computed using 800 m/s for EC8-A, 580 m/s for EC8-B, 270 m/s for EC8-C.

Figure 6 and Figure 7 show the comparison between prediction and observations for the geometrical mean of the horizontal and vertical components of PGA and PGV, respectively. The ASB14 coefficients for vertical ground motion are not available.

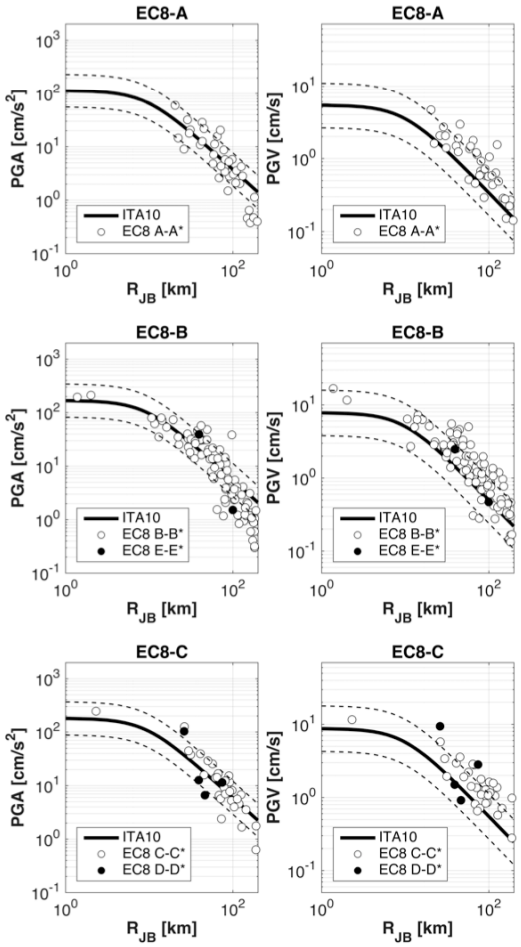

Figure 7. Observation vs. predictions for the vertical component. Left: PGA; right: PGV. Top: EC8 class A; middle: EC8 class B; bottom: EC8 class C.

On average, the observed horizontal PGAs match the predictions; higher values are observed for EC8-B in the distance range 50-100km; beyond 100km the observed ground motion attenuation with distance is faster than the predictions, especially for EC8-A and EC8-B soil categories. The near fault values are well predicted and they fall in the standard deviation range of the two GMPEs

considered. Observed horizontal PGVs (Figure 6) are generally higher than predictions, particularly for class EC8-B and EC8-C.
The observed vertical PGAs are well predicted up to 100km (Figure 7). For larger distances, the observations are lower than predictions, similarly to horizontal components. Observed vertical PGVs are, in general, higher than predictions (Figure 7).
The residuals (R_{es}) were calculated as logarithmic difference between observations and predictions and were decomposed in between-event δB_e (mean of residual per event) and within-event δW_{es} residuals ($\delta W_{es} = R_{es} - \delta B_e$), as proposed by Al-Atik et al. (2010).

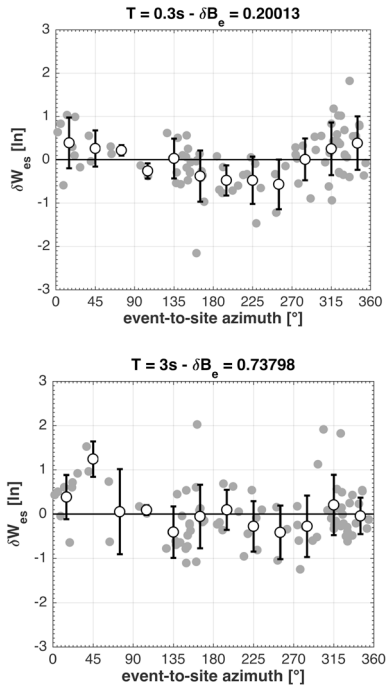

Figure 8. Within-event residuals δWes vs. azimuth for SA at T=0.3s (top) and 3s (bottom) for the stations within R_{JB}=80km. The event-to-site azimuth is computed clockwise from the north. The between-event value is reported in the title.

Figure 8 shows the within-event residuals against event-to-station azimuth, for the stations up to R_{JB}=80km. Positive residuals indicate under-predictions and are observed in the Northern sector at SA 0.3s (0-45° and 315-360°). Negative residuals (over-predictions) are instead obtained in the range 135-270°, corresponding to SW direction. This represents an additional evidence of directivity effects at high frequencies, as highlighted in Figure 4. No clear trend with azimuth is instead observed at SA 3s; large positive residuals are only observed for some stations located in alluvial basins (see also Figure 5). The between-event residual is found to be small at SA 0.3s, while it is larger and positive at SA 3s, which means a general under-prediction of the GMPEs at long periods.

IV. WAVEFORM FEATURES OF NEAR-FAULT STATIONS: AMT AND NRC

The near-fault recordings of AMT and NRC stations, both located at about 1.5 km from the fault projection but in opposite positions from the epicenter, present different characteristics in terms of peak values and frequency content.

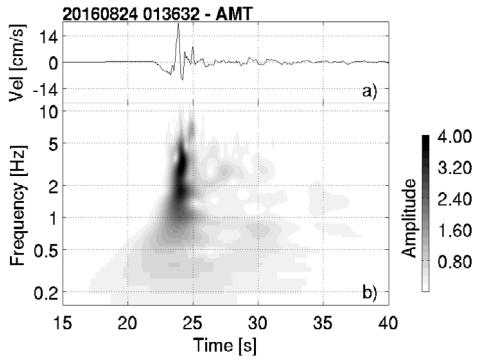

Figure 9. Velocity time history (a) and power spectrum (b) of the E component at station AMT

As shown in Figures 9a and 10a, the velocity time-series at AMT has a shorter duration compared to NCR (maximum significant duration T_{90}=3.8s vs. T_{90}=7.2s), and a higher energy content (Arias Intensity I_A=46cm/s

vs. I_A =32cm/s, evaluated as the largest value between the horizontal components).
The time–frequency analysis of these recordings (Pinnegar, 2006) allows us to identify arrivals and frequencies of different phases. The power spectrum of the horizontal velocity time series observed at AMT and NCR (Figure 10b and 11b) shows that both signals have large energy content in the frequency range 1-5 Hz in correspondence of the S phase. The lengthening of the NRC recording can be ascribed to subsequent arrivals of low frequency waves (about 1 Hz), due to 2D/3D site effects (Bindi et al, 2011b).

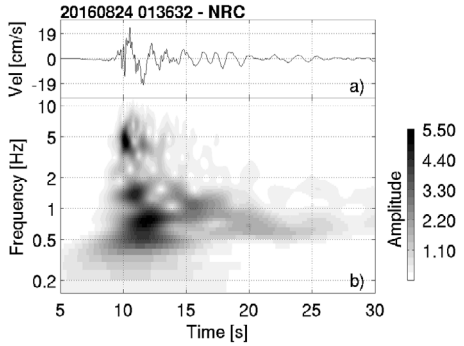

Figure 10. Velocity time history (a) and power spectrum (b) of the E component at station NRC

V. CONCLUSIONS

The recent earthquake of Amatrice (24/08/2016, M_W=6.0) was recorded by about 300 strong-motion stations. The accelerometric data were manually processed and are available at the ESM website (esm.mi.ingv.it).
The spatial distribution of the PGA and low period spectral ordinates show a pattern that can be related to the source-to-site azimuth. The residual analysis and the interpolation of observed data highlight the nature of the rupture, which is bilateral, dominated by the NW propagation. Different attenuation patterns are also evident towards West and East.
The vertical components are comparable to the horizontal ones only in the near-fault or when site/propagation effects contribute to increase the vertical components in the far field.
GMPEs generally fit the observations in the near-fault for low periods spectral ordinates; at distances larger than 80km, the residuals show a positive bias in the sense that the GMPEs tend to under-predict the observed ground motions. GMPEs for PGV and SA at long periods generally underestimate the observations, highlighting the necessity of reviewing the most recent GMPEs developed for Italy, widely based on analog records.

REFERENCES

Al Atik., L., Abrahamson, N., Bommer, J.J., Scherbaum, F., Cotton, F., and Kuehn, N. (2010) The variability of ground- motion prediction models and its components. Seismological Research Letters 81(5):794–801.

Akkar, S., Sandıkkaya, M. A., and Bommer, J. J. (2014). Empirical ground-motion models for point-and extended-source crustal earthquake scenarios in Europe and the Middle East. Bulletin of Earthquake Engineering, 12(1):359-387.

Bindi, D., Pacor, F., Luzi, L., Puglia, R., Massa, M., Ameri, G. and Paolucci, R. (2011a). Ground motion prediction equations derived from the Italian strong motion database. Bulletin of Earthquake Engineering 9:1899–1920.

Bindi, D., L. Luzi, S. Parolai, D. Di Giacomo, and G. Monachesi (2011b). Site effects observed in alluvial basins: the case of Norcia (Central Italy), Bulletin of Earthquake Engineering 9(6):1941–1959.

CEN (Comité Européen de Normalisation) (2004). Eurocode 8: design of structures for earthquake resistance – Part 1: general rules, seismic actions and rules for buildings, CEN, Brussels, www.cen.eu.

Davis, J.C. (1973). Statistics and Data Analysis in Geology. Wiley, New York.

Di Capua, G., Lanzo, G., Pessina, V., Peppoloni, S., Scasserra, G. (2011) The recording stations of the Italian strong motion network: geological information and site classification. Bulletin of Earthquake Engineering 9:1779–1796.

Di Giulio, G., A. Rovelli, F. Cara, R. M. Azzara, F. Marra, R. Basili, and A. Caserta (2003). Long-duration asynchronous ground motions in the Colfiorito plain, central Italy, observed on a two-dimensional dense array, Journal of Geophysical Research, 108(B10): 2486.

Luzi, L., Hailemikael, S., Bindi, D., Pacor, F., Mele, F., and Sabetta, F. (2008) ITACA (Italian ACcelerometric Archive): a web portal for the dissemination of italian strong-motion data. Seismological Research Letters, 79(5):716–722.

Luzi, L., Puglia, R., Russo, E., D'Amico, M., Felicetta, C., Pacor, F., Lanzano, G., Ceken, U., Clinton, J., Costa, G., Duni, L., Farzanegan, E., Gueguen, P., Ionescu, C., Kalogeras, I., Ozener, H., Pesaresi, D., Sleeman, R., Strollo, A. and Zare, M. (2016). The engineering strong-motion database: a platform to access Pan-European accelerometric data. Seismological Research Letters, 87(4):987-997.

Meletti, C., Galadini, F., Valensise, G., Stucchi, M., Basili, R., Barba, S., Vannucci, G., and Boschi, E. (2008). A seismic source zone model for the seismic hazard assessment of the Italian territory. Tectonophysics, 450(1):85-108.

Pacor, F., Paolucci, R., Luzi, L., Sabetta, F., Spinelli, A., Gorini, A., Nicoletti, M., Marcucci, S., Filippi, L., Dolce, M. (2011) Overview of the Italian strong motion database ITACA 1.0. Bulletin of Earthquake Engineering, 9(6):1723–1739.

Pinnegar, C. R. (2006). Polarization analysis and polarization filtering of three-component signals with the time–frequency S transform. Geophysical Journal International, 165:596–606.

ReLUIS-INGV Workgroup (2016). Preliminary study of Rieti earthquake ground motion records V5.0, http://www.reluis.it.

Tinti E., Scognamiglio L., Michelini A. and Cocco M. (2016). Slip heterogeneity and directivity of the ML 6.0, 2016, Amatrice earthquake estimated with rapid finite-fault inversion. Geophysical Research Letters (submitted).

Wald, D. J., and Allen, T. I. (2007). Topographic slope as a proxy for seismic site conditions and amplification. Bulletin of the Seismological Society of America, 97(5):1379-1395.